Bioaccumulation, biodistribution, and transformation of polyvinylpyrrolidone-coated silver nanoparticles in edible seaweeds

Monica Quarato, Laura Rodriguez-Lorenzo, Ivone Pinheiro, Juan José López-Mayán, Mick Mackey, Antonio Moreda-Piñeiro, Miguel Spuch-Calvar, Julie Maguire, Pilar Bermejo-Barrera, Miguel A. Correa-Duarte, Begoña Espiña

PII: S0048-9697(24)05064-2

DOI: https://doi.org/10.1016/j.scitotenv.2024.174914

Reference: STOTEN 174914

To appear in: *Science of the Total Environment*

Received date: 22 March 2024

Revised date: 16 July 2024

Accepted date: 18 July 2024

Please cite this article as: M. Quarato, L. Rodriguez-Lorenzo, I. Pinheiro, et al., Bioaccumulation, biodistribution, and transformation of polyvinylpyrrolidone-coated silver nanoparticles in edible seaweeds, *Science of the Total Environment* (2024), https://doi.org/10.1016/j.scitotenv.2024.174914

Bioaccumulation, Biodistribution, and Transformation of Polyvinylpyrrolidone-coated Silver Nanoparticles in Edible Seaweeds

Monica Quarato[1], Laura Rodriguez-Lorenzo[1,*], Ivone Pinheiro[1], Juan José López-Mayán[2], Mick Mackey[3], Antonio Moreda-Piñeiro[2], Miguel Spuch-Calvar[4], Julie Maguire[3], Pilar Bermejo-Barrera[2], Miguel A. Correa-Duarte[4], Begoña Espiña[1,*]

1. *INL - International Iberian Nanotechnology Laboratory, Avda. Mestre Jose Veiga s/n, Braga, Portugal*
2. *GETEE - Trace Element, Spectroscopy and Speciation Group, Institute of Materials iMATUS, Department of Analytical Chemistry, Nutrition and Bromatology, Faculty of Chemistry, Universidade de Santiago de Compostela, Avenida das Ciencias, s/n., 15782, Santiago de Compostela, Spain*
3. *Indigo Rock Marine Research, Gearhies, Bantry, Co. Cork, P75 AX07*
4. *CINBIO, Universidade de Vigo - Campus Universitario Lagoas Marcosende, 36310, Vigo, Spain*

*Corresponding authors: L.R.-L.: laura.rodriguez-lorenzo@inl.int and B.E.: begona.espina@inl.int

KEYWORDS: AgNPs, *Palmaria palmata*, *Ulva fenestrata*, electron microscopy, biodistribution, NP transformation.

Abstract

Seaweeds are recognised as a potential eco-friendly food source. However, some species have shown the capacity to bioaccumulate many substances of diverse nature, such as inorganic nanoparticles (NPs), which may have potentially harmful effects on them. Among these NPs, silver nanoparticles (AgNPs) have been used to enhance the antifungal and antibacterial properties of the final consumer products, such as textiles and food packages. Their potential release into the aquatic environment raises significant concern, increasing the probability of interaction with aquatic biota, such as macroalgae.

In this work, we investigated the differences in bioaccumulation, biodistribution, and transformation of NPs as a function of seaweed species. We selected polyvinylpyrrolidone-coated silver nanoparticles (PVP-AgNPs) as model NP since they remain colloidally stable in seawater, focusing the study only on single particles and not on aggregates. The study was conducted on two different seaweed species with high commercial interest and value as human food: the red seaweed *Palmaria palmata* and the green seaweed *Ulva fenestrata*. Single-particle inductively coupled plasma mass spectroscopy (spICP-MS) analysis showed high and similar bioaccumulation of PVP-AgNPs in both seaweeds, in the range of 10^9 NPs/g of seaweed. However, electron microscopy with energy-dispersive X-ray analysis demonstrated that their time-dependent distribution and transformation in the algal tissue, mainly dissolution and formation of sulfur-rich corona and/or sulfidation, highly depended on the seaweed type.

These results indicate that special attention should be given to the presence and transformation of AgNPs in seaweeds intended for human consumption. Not only the dissolution degree but also the speciation of these NPs could heavily impact their bioaccessibility, bioavailability, biodistribution, and toxicity to humans after ingestion.

Introduction

The increasing fraction of nanomaterials' production, including inorganic nanoparticles (NPs), has led to a high probability of their release into the environment, which raises concern about the fate and the effect of these nanomaterials due to their possible interaction with living organisms (Zhou et al., 2016). As a consequence of their extensive applications and broad commercialisation (Chernousova and Epple, 2013), silver NPs (AgNPs) may have a high potential impact on marine ecosystems, posing a health risk not only to aquatic organisms and plants (Blinova et al., 2013) but also to humans (Kose et al., 2023). Recent studies have revealed significant levels of Ag and AgNPs in water, sediments, plants, and fishes, where higher levels of accumulation are reached (e.g., 9.14 and 53.78 mg/kg of Ag) (Huang et al., 2022; Mat Lazim et al., 2023; Niu et al., 2023). Filter-feeding molluscs (i.e., marine mussels, oysters) are particularly affected, suffering oxidative stress, alteration in enzymatic activity, and cellular damage because of their exposure to those NPs or their dissolved ions (Calisi et al., 2022; Gonçalves and Bebianno, 2023; Sadri and Khoei, 2023; Zhang and Wang, 2023). Li and Cummins developed a semi-quantitate risk ranking for human health assessment of engineered nanomaterials, highlighting that AgNPs present the highest health concern by exposure via natural water sources. They predicted an environmental concentration of total silver in the range of ng/L in surface waters (Li and Cummins, 2021). Although wastewater treatment plans have reported a high removal efficiency for AgNPs at a concentration range of µg/L – ng/L (82 – 97%) (Li et al., 2016; Nabi et al., 2021), the estimated annual release in the effluent was still high (around 33 Kg of AgNPs) (Li et al., 2016). However, determining the concentration level of these NPs in marine environments remains a challenge because their behaviour is highly influenced by aggregation/agglomeration, dissolution, and formation of eco-corona, which increase the uncertainty in their suspended concentration and consequently, their accessibility to the marine biota (Calisi et al., 2022).

Fully exploited in Asian countries, seaweeds are commonly consumed as human food in many parts of the world representing one of the possible solutions to feed the growing human population (Parodi et al., 2018). Seaweed aquaculture (land-based and at sea) is developing in several countries in Europe (top 3: France, Ireland, and Spain) and it already represents 32% of the macroalgae production

platforms (Araújo et al., 2021). Specifically, *Palmaria palmata* (*P. palmata*), also known as red seaweed dulse, is one of the most popular species used for human consumption in Europe. rance is the biggest producer, with an annual production of 138 - 458 tons (WW), generating 90% of the *P. palmata* consumed in Europe in 2013 (Stévant et al., 2023). In contrast, *Ulva* spp., known as sea lettuce, has recently raised interest due to its extraordinary nutritional properties, high productivity, and high environmental tolerance, even though < 0.1% of the total seaweed production is related to green seaweed (Steinhagen et al., 2021).

Despite the many benefits, such as high availability, low cost, and simple cultivation methods, there is a growing concern about risks associated with contaminants accumulation in seaweed (Bouga and Combet, 2015). Not surprisingly, macroalgae can interact and absorb or adsorb many components dissolved or/and suspended in water bodies and rapidly respond to them. They are considered a sound biomonitoring system and, being at the lowest level of the aquatic food chain, these interactions can pose a risk for the whole aquatic ecosystem and ultimately to humans (Gökçe, 2016) (Dhargalkar and Verlecar, 2009).

Several studies have investigated the toxicity of dissolved metals in marine ecosystems, but very few articles have addressed the potential risk of these metals in their nano-sized form (Giusti, 2001) (Peng et al., 2022). Among them, Turner et al. investigated the toxicity of AgNPs in the marine macroalgae *Ulva lactuca* by monitoring the photosystem II (Turner et al., 2012). Unfortunately, these studies have not tackled the potential internalisation and distribution of these NPs in their tissues to understand better their correlation and impact on the toxicity responses observed.

Identifying and localising AgNPs within tissues is challenging due to their small size and the possible transformations that these NPs can undergo within the algae. Oxidation processes (i.e., dissolution) that lead to the release of ionic silver, size reduction, and complexation processes with chloride or sulfide can completely modify the NP physicochemical properties, which could induce drastic changes in their acute toxicity and kinetics mechanisms, influencing NP's bioavailability (Jorge de Souza et al., 2019).

Thus, electron microscopy (EM) and more specifically transmission EM (TEM) is an excellent tool to investigate these processes since they offer a resolution of a few nanometers in conventional TEM and

even atomic resolution by using aberration-corrected high-resolution TEM (HRTEM) (Plascencia-Villa et al., 2016). Moreover, TEM allows visualisation and localisation of electron-dense NPs in the tissue without any specific labelling or *a priori* information about their composition. TEM can also estimate the number of particles inside specific tissues' compartments (e.g., cell wall, and cell membrane). High-angle annular dark-field scanning transmission EM (HAADF STEM) coupled with energy dispersive x-ray spectroscopy (EDX) can extract more information not only in terms of the ultrastructure of the tissue without extra post-staining on the grid, by acquiring high contrast images, but also regarding NP composition, which may open the opportunity of studying NP transformation within the tissue (López-Mayán et al., 2023; Zimmermann et al., 2023). The integration of EDX analysis also allows for the discrimination between electron-dense NPs that could be found in real samples by elemental chemical composition (Scimeca et al., 2018). Some publications have reported the use of TEM for the localisation of AgNPs in the tissue of different organs, such as gills and liver, but not always the NPs were identified by EDX analysis (García-Alonso et al., 2011; Jang et al., 2014; Meng et al., 2014; Zhou et al., 2019). Despite all the advantages offered by EM coupled to EDX analysis, and to the best of our knowledge, no investigation has explored the potential biodistribution and transformation of AgNPs in seaweed by EM coupled with EDX. There is limited research concerning the analysis of AgNPs' interaction with terrestrial plants, but nothing available focuses on macroalgae. Stegemeier et al. analysed the biodistribution of Ag_2S NPs and AgNPs in alfalfa (*Medicago sativa*) roots by TEM, localising both NPs in the cell wall (Stegemeier et al., 2015). Cvjetko et al. confirmed the AgNPs uptake by root cells of tobacco (*Nicotiana tabacum*) using TEM coupled with EDX (Cvjetko et al., 2018). However, the possible transformations of AgNPs (i.e., without previous extraction of the NPs from the tissue) have not been studied directly in the tissue by EM and EDX to the best of our knowledge.

Thus, this work aimed to investigate the biodistribution and transformation of commercially available polyvinylpyrrolidone-coated silver nanoparticles (PVP-AgNPs) into two distinct species of seaweed used as human and animal food, *U. fenestrata* and *P. palmata*, by conventional TEM, high-resolution TEM (HRTEM), and HR scanning TEM (HRSTEM) coupled with EDX.

Materials and Methods

Silver Nanoparticles (AgNPs). Commercial self-dispersed 15 nm AgNPs were supplied by SSNano (Houston, TX, USA; product code: 0127SH). The powder, composed of 25% wt silver and 75% wt polyvinylpyrrolidone (PVP), was dispersed in ultrapure water with a resistivity of 18.2 MΩ at 25 °C (Millipore apparatus, MQ Aquantage A10, Merck, Algés, Portugal) and sonicated for 15 min using a bath sonicator (Elmasonic P, Elma, VWR, Amadora, Portugal) (37 kHz, 100% at 25 °C).

AgNPs were fully characterised by UV-Vis spectroscopy (Perkin-Elmer LAMBDA 950 spectrophotometer, Scientific Laboratory Supplies, Wilford, Nottingham, UK), dynamic light scattering (DLS) for hydrodynamic size/zeta potential analysis (SZ-100 device, Horiba, ABX SAS, Amadora, Portugal) and transmission electron microscopy (JEOL JEM 1010 transmission electron microscope operating at 100 kV, Izasa Scientific, Madrid, Spain). The stability of the particles at the concentration of 12.5 mg/L was assessed in both ultrapure water and reconstituted seawater. The reconstituted seawater (RSW) with a salinity of 35‰ was prepared by adding 14 Kg of marine salt to 400 L of deionised water. The salt was left to dissolve for 6 h, and then the final adjustments to the salinity were made through the addition of either deionised water or additional salt, as needed. Final composition included Na^{+}, Mg^{2+}, K, Ca^{2+}, Sr^{2+}, Rb^{2+}, Fe, Li^{+}, Cl^{-}, SO_4^{2-}, Br^{-}, F^{-}, and B. The water was maintained in a glass tank with strong aeration, and in recirculation at 20 °C until it was collected for particle spiking. The pH and conductivity were maintained at 7.7 – 8.1 and 47.3 mS/cm, respectively.

The UV-Vis analysis of the dissolution of these NPs in both media was carried out by taking aliquots of 1 mL from 500 mL of 12.5 mg/L PVP-AgNPs dispersion after 0, 1, 2, 3, 4, 5, 6, 7, 14, 21, and 28 days of incubation. The aliquots were loaded into a quartz cuvette, 10 mm optical path, to perform the UV-Vis analysis.

Bioaccumulation assay. Two independent experimental bioaccumulation assays, one for *P. palmata* and another for *U. fenestrata*, were performed at Indigo Rock Marine Research Station (Cork, Ireland). The exposure dose of PVP-AgNPs was 1 mg/L of Ag. Seaweeds were cultivated in 40 L tanks at a temperature of 16 ± 1 ºC, with 12 hours of white light and 12 hours of darkness. The

acclimation was carried out by placing 400 g of wet, fresh seaweed into 40 L of seawater for ten days. The day before each assay, 100 g of the least healthy-looking seaweed was removed, reducing the total mass to 300 g of seaweed per tank. The growth promotion and feeding of the seaweed were carried out using cell-HI F2P medium (Varicon Aqua), a soluble nutrient blend commonly used in marine macroalgae production.

Parameters like pH, temperature, dissolved O_2, and salinity were measured daily, while conductivity, ammonium, and nitrites were tested twice per week. These parameters remained stable during assays: the temperature was 15 ± 1 ºC, photosynthetically active radiation (PAR) was 40 – 60 $\mu mol \cdot s^{-1} \cdot m^{-2}$, the pH and nitrate concentration were maintained at 8.1 and 6.62×10^{-4} M, respectively. **Figure 1C** schematically describes the experimental design of the bioaccumulation assay. Both *P. palmata* and *U. fenestrata* were exposed to PVP-AgNPs with a concentration of 1 mg/L of Ag (the corresponding PVP was 3 mg/L since the ratio PVP:Ag in the composite was 3:1 *wt*) every 7 days. The total experiment duration was 28 days. For each of the assays, two different controls were included: growing medium without NPs and growing medium with 3 mg/L of PVP alone. Three tanks per treatment group were included in each assay (total tanks: 9). Three times per week, 30 mL (0.1 g/mL) of F2 growing medium containing the phytoplankton was added. Fifty per cent of the water was replaced twice per week, two days before and two days after the addition of PVP-AgNPs. The water was fully renewed once per week, adding F2 medium with PVP-AgNPs to reach a final concentration of 1 mg/L in 40 L. In this way, the only PVP-AgNPs remaining from the previous dosage were the ones in close interaction with the seaweed.

Seaweed samples were collected on days 0, 7, 14, 21, and 28 for analysis by ICP-MS and electron microscopies. Three replicate samples were taken from each tank and each trial for ICP-MS analysis. Each seaweed sample was washed with ultrapure water to remove salts and contaminants from the seawater. Then, the samples were frozen until ICP-MS analysis.

In the case of electron microscopy analysis, two seaweed samples were taken for each species from each treatment group after every exposure time. The seaweed blade leaf was cut into 0.7 cm squared fragments and fixated overnight at 4 ºC using the Karnovsky fixative solution (a mixture of 2%

paraformaldehyde and 2.5% glutaraldehyde in 0.1 M sodium cacodylate buffer) for organelles preservation. These fragments were stored at 4 ºC under shaking until the sample preparation for electron microscopy analysis was completed.

Quantification of total silver and AgNPs by ICP-MS and spICP-MS. Wet seaweed samples were manually crushed, homogenised, and stored in polyethylene tubes at -18.0 ºC until microwave acid digestion and enzymatic extraction of AgNPs were performed. The quantification of total silver element and AgNPs in crushed seaweed was carried out by ICP-MS/spICP-MS with a NexION 2000 ICP-MS (Perkin Elmer, Waltham, MA, USA). The operating conditions are described in the supporting information in **Table S1**.

A microwave-assisted acid digestion method was established to extract the total silver from the seaweed matrix. The reaction mixture involving 1 g of crushed seaweed, 4 mL of ultrapure water, 3 mL of HNO_3 69% (w/w), and 1 mL of H_2O_2 33% (w/v) was added in a Teflon vessel. The seaweed samples were digested using Ethos Plus microwave lab station (Milestone, Bergamo, Italy) at 200 ºC and 800 W power following: 1) temperature ramp from room temperature (RT) to 90 ºC in 4 min, 2) temperature ramp from 90 to 140 ºC in 5 min, 3) temperature ramp from 140 to 200 ºC in 5 min, 4) hold time 20 min at 200 ºC and 5) cooling step to RT. The digests were then diluted with ultrapure water up to 25 mL before their analysis by ICP-MS. Two blanks were prepared for each set of experiments.

Enzymatic hydrolysis in combination with ultrasonication of the samples used for AgNPs extraction was previously published (López-Mayán et al., 2022). Briefly, 50 mg of seaweed sample were placed into a 10 mL polyethylene tube and dispersed in 7 mL of 2 mM citrate buffer pH 4.5. The suspension was sonicated in an ice bath using 20% amplitude, 1 s pulse on and 1 s pulse off for 5 min. After sonication, 2 mL of 25 g/L Macerozyme R-10® (Merck, Darmstadt, Germany) solution was added and the mixture was incubated for 6 h at 37 ºC under shaking (150 rpm). The final extracts were filtered using 5.0 µm cellulose syringe filters and then diluted with 1% (v/v) glycerol before spICP-MS analysis. Sample introduction flow rate and transport efficiency (TE%) were calibrated and measured before each measurement set using 49.6 nm AuNPs (NanoComposix material) at a

concentration of 9.89×10^4 NPs/mL in ultrapure water. TE% was automatically calculated by using the SyngistixTM Nano Application software. Under the same instrumental conditions as those used for Ag, but monitoring m/z 197 for Au, the obtained TE% was within the 8.8-11.5% range. Finally, measurements were carried out by using ionic Ag aqueous standards from 0 to 5 (Ag) μg/L. The concentration of AgNPs/mL and size distribution were automatically calculated by SyngistixTM Nano Application software.

Electron microscopy analysis. The fixated samples were processed using an EM TP Tissue processor (Leica microsystems) for EM analysis. Briefly, osmium tetroxide solution at 1% (Science Services, Munich, Germany) was used for the post-fixation step to stain lipids. The fragments were then dehydrated by sequential washings using water:ethanol mixtures, increasing the ethanol fraction up to 100%, and with propylene oxide. Propylene oxide was also used for the gradual impregnation of the fragments with the epoxy resin (EMBed-812 kit, Science Services, Munich, Germany). The fragments were then placed in silicone moulds with resin and left to cure for three days at 60 ºC. Ultrathin sections (≈ 80 nm thick) were obtained using a PowerTome PC ultramicrotome (RMC Boeckeler, USA) with a diamond knife (Diatome) and placed on 100 mesh titanium grids. The bioaccumulation analysis of PVP-AgNPs was performed by TEM. TEM images at low magnification of each section were acquired with a JEOL JEM 1010 transmission electron microscope operating at 100 kV. The analysis of their identification and transformation was carried out by high-resolution TEM (HRTEM) and HR scanning TEM (HRSTEM) coupled with EDX using FEI Titan (G3) Cubed Themis 60-300 kV, operating at 60 kV. STEM images were acquired using a high-angle annular dark-field (HAADF) detection. EDX maps were acquired for 20 min, using a Super-X detector system involving four windowless silicon drift detectors, which enhance the acquisition efficiency and spatial resolution. The ratio Ag and S analysis was carried out using Velox Software (Thermo Fisher) by selecting the area of the corresponding NP (i.e., the bright spot observed in the STEM image).

Results and Discussion

We comprehensively characterised the PVP-AgNPs used in the study in terms of size and colloidal stability. **Figure 1A, Figure S1A and B, and Figure S2A** show representative TEM images of the

particles dispersed in reconstituted seawater (RSW) and ultrapure water, which reveal that AgNPs have a spherical shape with an average primary diameter of 24.8 ± 6.5 nm and 24.7 ± 6.4 nm in both media (histograms in **Figure 1A and Figure S2A**), demonstrating that these NPs presented similar size in RSW and ultrapure water immediately after being dispersed in both media. We assessed their colloidal stability in RSW since it is well-known that NPs tend to form aggregates in high salt-contained media and this may have an impact on the interaction (i.e., adsorption, and cell uptake) with the marine organisms, in this case seaweeds (Moore et al., 2015). **Figures S2C and D** show the analysis by UV-Vis spectroscopy, dynamic light scattering (DLS), and zeta potential. PVP-AgNPs were colloidally stable in RSW since we did not observe either a red-shift of the localised surface plasmon resonance (LSPR) band of the AgNPs (**Figure S2C**) or an increase in the hydrodynamic size (**Figure S2D**). We previously studied the colloidal stability of these AgNPs in RSW over 1 month (Quarato et al., 2021), demonstrating that the medium, i.e. reconstituted marine water, had not a substantial impact on their colloidal stability in terms of aggregation at the concentration studied during the bioaccumulation assay. As these PVP-AgNPs did not tend to form aggregates in RSW, we could study their possible dissolution by UV-Vis spectroscopy, as reported previously by (Sikder et al., 2018). **Figure S3** shows UV-Vis spectra of PVP-AgNPs dispersed in both ultrapure water and RSW acquired after 0, 7, 14, 21, and 28 days of incubation. LSPR underwent a slightly blue shift and decreased in intensity after 7 days of incubation, demonstrating that these NPs were partially dissolved in both media. TEM analysis after 7 days of incubation in both media showed a variation in the mean of the diameter and the size distribution, as shown in the histograms in **Figure 1B** for RSW and **Figure S2B** for ultrapure water. In both media, the AgNPs remained spherical (**Figure 1B**, **Figure S1C,** and **D** and **Figure S2B**); however, the average size decreased by 1.2 nm in ultrapure water, 23.6 ± 7.0 nm, while it increased by 1.3 nm in RSW, 26.0 ± 6.2 nm. As reported previously, the increase in size of AgNPs in RSW can be explained by the reduction of the dissolved Ag^{+1} onto the existent AgNPs (Zou et al., 2017).

To better understand the percentage of dissolution, we plotted the percentage of Ag dissolution against the time of incubation. The percentage of Ag dissolution was calculated using the approximation previously reported (Sikder et al., 2018):

$$\%\, Ag\ dissolution = \left(\left(Abs_0^{LSPR} - Abs_t^{LSPR} \right) \Big/ Abs_0^{LSPR} \right) \times 100$$

Where Abs_0^{LSPR} and $Abs_t^{LSPR}$is the absorbance at LSPR at time 0 and at different incubation times, respectively. **Figure S3E** shows that dissolution of AgNPs reached a plateau after 14 days of incubation in both media being 35 ± 6% for RSW and 23 ± 10% for ultrapure water. The dissolution rate of these PVP-AgNPs was lower than the ones previously reported. The lower dissolution observed here could be explained by the higher efficiency of the PVP shell to protect the Ag surface against oxidation (Kyrychenko et al., 2015). We estimated the thickness of the PVP shell around AgNPs by the difference between the size calculated by electron microscopy and the hydrodynamic size obtained by DLS. The thickness estimated for PVP-AgNPs studied here was 12.5 nm, while the thicknesses calculated for PVP-coated AgNPs reported previously were smaller: 2.2 nm, 8.5 nm, and 5 nm for the NPs studied by (Sikder et al., 2018), (Tejamaya et al., 2012), and (Zhao et al., 2021), respectively. The dissolution percentage after 5 days of incubation observed by (Sikder et al., 2018) was higher, ~ 88% and ~ 63% in 20 ppt RSW and 20 ppt natural seawater, respectively, for 0.1 mg/L PVP-AgNPs with a PVP layer with a thickness of 2.2 nm after 5 days incubation, than in our study, which was 22% in 35 ppt RSW for 1 mg/L PVP-AgNPs with a PVP layer with a thickness of 12.5 nm. However, a similar percentage of dissolution, ca. 30 % was reported by Zhao et al. after 7 days of incubation of 1 mg/L PVP-AgNPs with a PVP layer with a thickness of 5 nm in 0.3 M NaCl salt water (Zhao et al., 2021). In the present study, the dissolution after 7 days of incubation was 24% in 35 ppt RSW (the concentration of chlorides was 0.5 M). This finding demonstrates that a higher grafting coverage of the Ag surface by PVP molecules has a substantial impact on the dissolution rate since this high-dense PVP layer reduces the water penetration (Kyrychenko et al., 2015) and, therefore, the diffusion of oxygen and chlorides close to the Ag surface.

After studying the colloidal stability and dissolution of the selected PVP-AgNPs, we performed the bioaccumulation assay by exposing two seaweeds, *U. fenestrata and P. palmata*, to these NPs over 28

days (**Figure 1C)**. The Materials and Methods section describes the detailed exposure conditions and analysis. We analysed the bioaccumulation by single-particle inductively coupled plasma mass spectroscopy (spICP-MS) and the biodistribution and NP transformation by TEM and STEM-EDX after 0, 7, 14, 21, and 28 days of exposure.

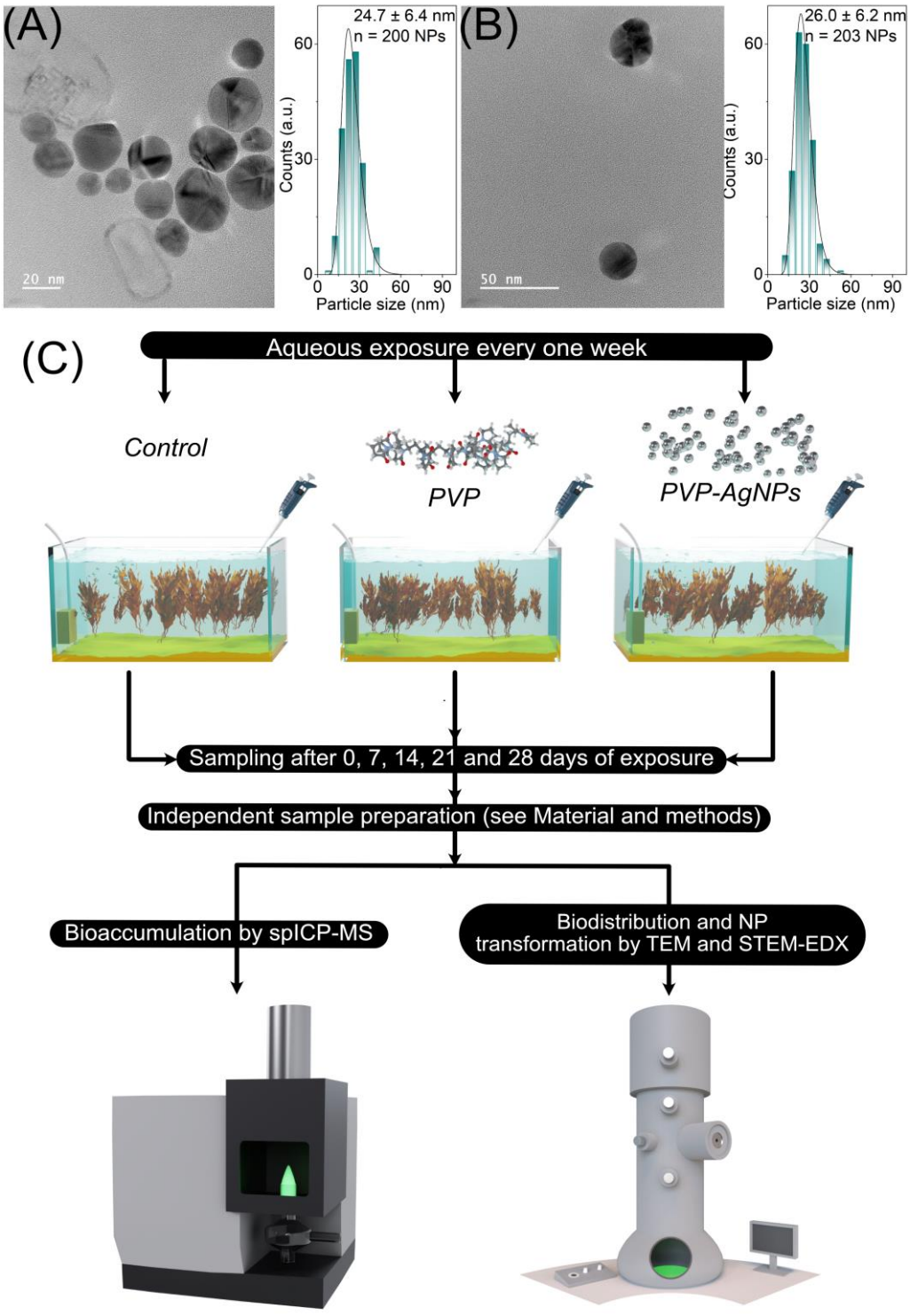

Figure 1. Representative TEM images and their histograms of selected PVP-AgNPs after (A) 0 days and (B) 7 days of incubation in RSW seawater. In the bioaccumulation assays, both seaweeds were exposed to PVP alone at a concentration of 3 mg/L, which is the concentration present in PVP-AgNPs, and PVP-AgNPs at a concentration of 1 mg/L of Ag and 3 mg/L of PVP over 28 days. A control was included in the assay. All treatment groups (i.e., control, PVP, and PVP-AgNPs) were analysed by spICP-MS and EM techniques. The illustrative scheme of the assay is shown in (C).

To investigate any possible morphological change in the seaweed' tissue, we acquired and analysed TEM images of 1) PVP-AgNPs-exposed seaweeds' blades, 2) seaweeds' blades exposed to 3 mg/L PVP alone to study the possible effect of the NP coating and 3) non-exposed seaweeds´ blades that acted as a control, after 0 and 28 days of exposure. **Figures S4** and **S5** show the TEM images for *P. palmata* and *U. fenestrata* respectively. Both seaweeds have very different blade cellular ultrastructure and tissue organisation. *P. palmata* presents larger cells in the central axis surrounded by several layers of smaller cortical cells not organised in lines. While *U. fenestrata* blade organisation consists of two polarised (chloroplast facing the apical/external side) lines of cells where the two layers are easily differentiated. No evident difference in the structural organisation of the cells was observed between treatment groups and exposure time analysed, indicating that both seaweeds were not damaged or significantly disturbed by the exposure conditions.

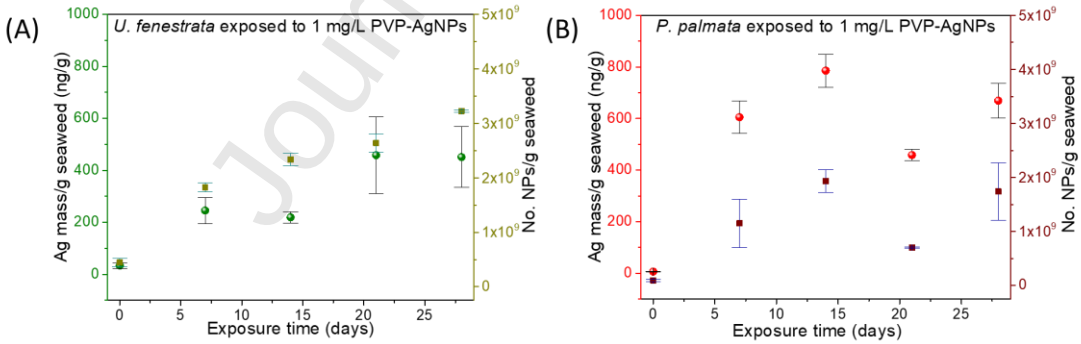

Figure 2. Total silver (Ag mass/g of seaweed) and silver nanoparticles (No. NPs/g of seaweed) bioaccumulation in (A) *U. fenestrata* and (B) *P. palmata* exposed to 1 mg/L PVP-AgNPs at different exposure times.

After confirming that both seaweeds did not undergo evident structural adverse effects when exposed to PVP-AgNPs, we investigated the NP' bioaccumulation by spICP-MS. The extraction of AgNPs from the selected seaweeds was previously optimised to avoid any modification on the size

distribution and colloidal stability of the nanoparticles (López-Mayán et al., 2022). This extraction is based on ultrasonication followed by enzymatic hydrolysis using Macerozyme R-10 (experimental details in Materials and Methods section), showing a good repeatability, sensitivity, and analytical recovery of the extracted AgNPs for spICP-MS measurements. **Table S2** shows the total silver measured by ICP-MS in *U. fenestrata* and *P. palmata* after being exposed to 0 mg/L PVP-AgNPs (i.e., control), 3 mg/L PVP-40K and 1 mg/L PVP-AgNPs. The two seaweeds contained a slight amount of ionic silver in both control' and PVP' treatment groups as well as in PVP-AgNPs at 0 days of exposure. The presence of Ag in seaweed sampled in Ireland was already reported, and the values detected in this study are within the previously analysed range. (Jönsson and Nordberg Karlsson, 2024). The concentration of total silver only increased in the treatment group exposed to 1 mg/L of AgNPs every 7 days, as expected (**Table S2**). Interestingly, the results showed that similar amounts of AgNPs per gram of seaweed, in the range of 3×10^9 – 1×10^9 NPs/g, were estimated and these numbers of NPs, either internalised or externally associated, remained constant from 7 days to 28 days of exposure (**Figure 2**, square dots). However, the total ionic silver quantified by ICP-MS was significantly higher in *P. palmata* (669 – 786 ng/g) than in *U. fenestrata* (246 – 459 ng/g) (**Figure 2**, sphere dots and **Table S2**). These values were 38-fold lower than the "no observable adverse effect level" (NOAEL) in the liver in rats (i.e., 30 µg/g) previously reported (Kim et al., 2010). Also, the AgNPs studied in this previous report had a bigger size (i.e., 56 ± 2 nm), which could influence the NOAEL estimated because it is well-known that smaller particles present higher toxicity response at lower concentrations (Liu et al., 2019). In line with this, it has been reported that concentrations down to 200 ng/g of AgNPs provoked observable adverse effects in the gastrointestinal tract (Qi et al., 2023).

We calculated the corresponding AgNPs per gram using the total silver values and the size determined by spICP-MS (the Table included in **Figure S6**). The values obtained showed a clear difference between the seaweed species. The calculated NPs/g values for *U. fenestrata* were like the ones experimentally obtained, being only slightly higher in the last two exposure times (i.e., 21 and 28 days, **Figure S6A**). However, in the case of *P. palmata*, the calculated NPs/g values were higher than the experimental ones at all time points (**Figure S6B**). These differences can be attributed to 1) A

fraction of AgNPs were smaller than the limit of detection of spICP-MS (LOD_{size} = 14 nm) and thus not detected in single particle mode and/or 2) AgNPs underwent dissolution when they were associated/internalised in the seaweeds' tissue. Both explanations can be supported since the sizes obtained by spICP-MS (Table in **Figure S6**), between 24 – 30 nm, were smaller than the initial hydrodynamic size, 47 nm (**Figure S2D**). Moreover, this transformation was stronger in *P. palmata* than in *U. fenestrata.*

Additionally, an abrupt decrease in the accumulation (~460 ng/g) of both total silver and AgNPs in *P. palmata* after 21 days of exposure was observed (**Figure 2** and **Table S2**). A recovery of the accumulation (~670 ng/g) was detected at 28 days of exposure. Similar behaviour has been observed in the bioaccumulation of metals by other seaweeds, such as *Gracilaria lemaneiformis.* The accumulation rate decayed after 15 and 21 days of exposure and subsequently, the metal concentration increased after 28 days of exposure (Wang et al., 2014). This tendency may be explained by the balance between accumulation and detoxification processes. Phytochelatins, plant' homologous for metallothioneins, are a class of heavy-metal-binding peptides, which are synthesised upon exposure to many different heavy metals, including Ag (Grill et al., 1987). Thus, above a certain level of accumulation of AgNPs, detoxification mechanisms may be triggered by synthesising phytochelatins and inducing strong depuration via cell or tissue compartmentalisation (Seregin and Kozhevnikova, 2023), promoting a decrease in the total concentration of both ionic and particulate of these NPs.

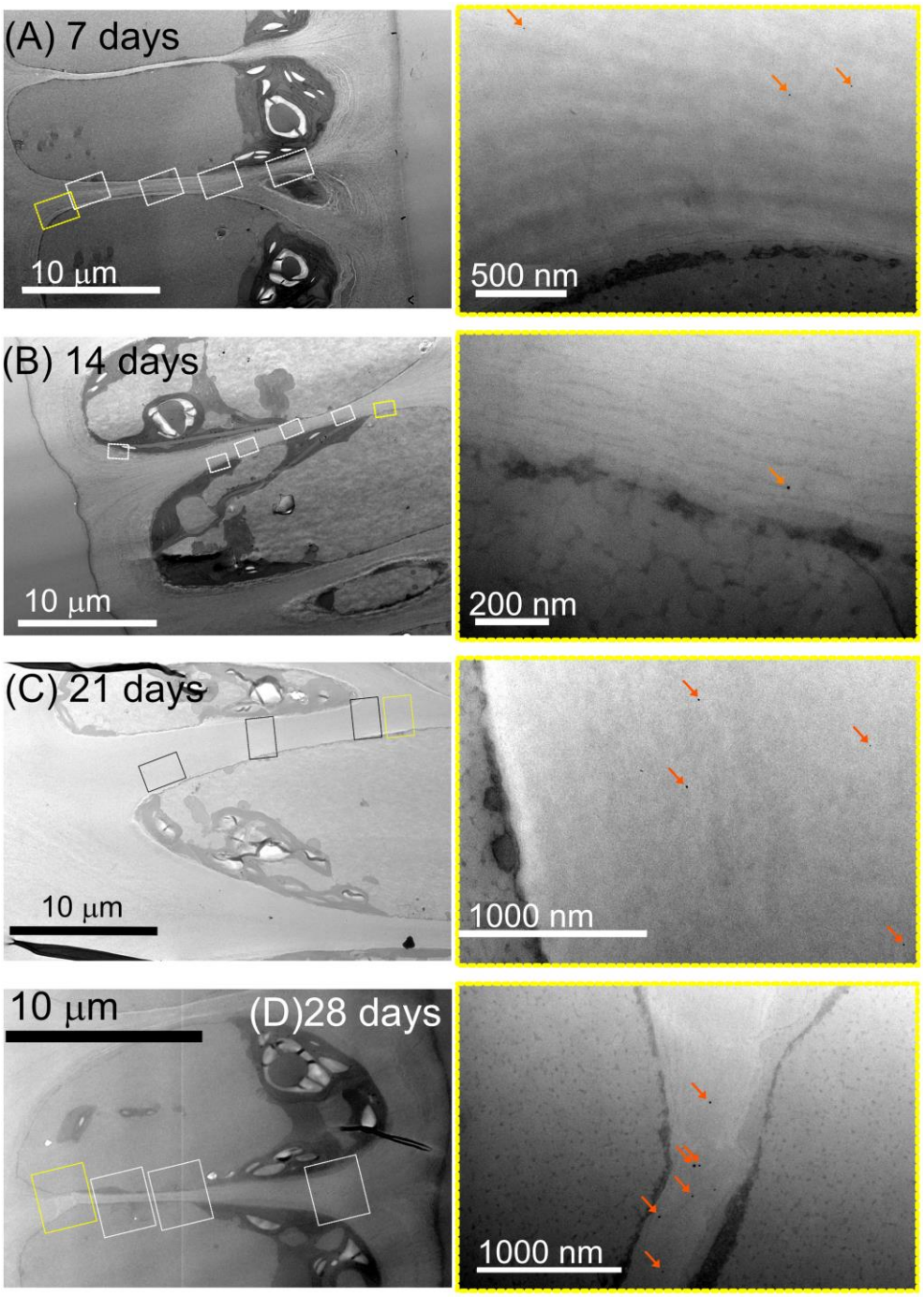

Figure 3. Biodistribution of PVP-AgNPs in *U. fenestrata* after (A) 7, (B) 14, (C) 21, and (D) 28 days of exposure. The different squares in the lower magnification TEM images (left) indicate the tissue's positions analysed at higher magnification. TEM images acquired in the area framed by yellow squares are shown on the right panel, which shows the deepest localised AgNPs in the tissue at each time point. The rest of the TEM images at a higher magnification acquired into the area framed by white (7, 14, and 28 days) and black (21 days) squares can be found in the supporting information: Figure S7 for 7 days of exposure; Figure S9 for 14 days of exposure; Figure S12 for 21 days of exposure and Figure S14 for 28 days of exposure. The orange arrows indicate the position of the localised AgNPs. TEM images shown in (C) and (D) were processed by merging 4-6 individual TEM images at the same magnification using Affinity Photo (version 1.10.5.1342).

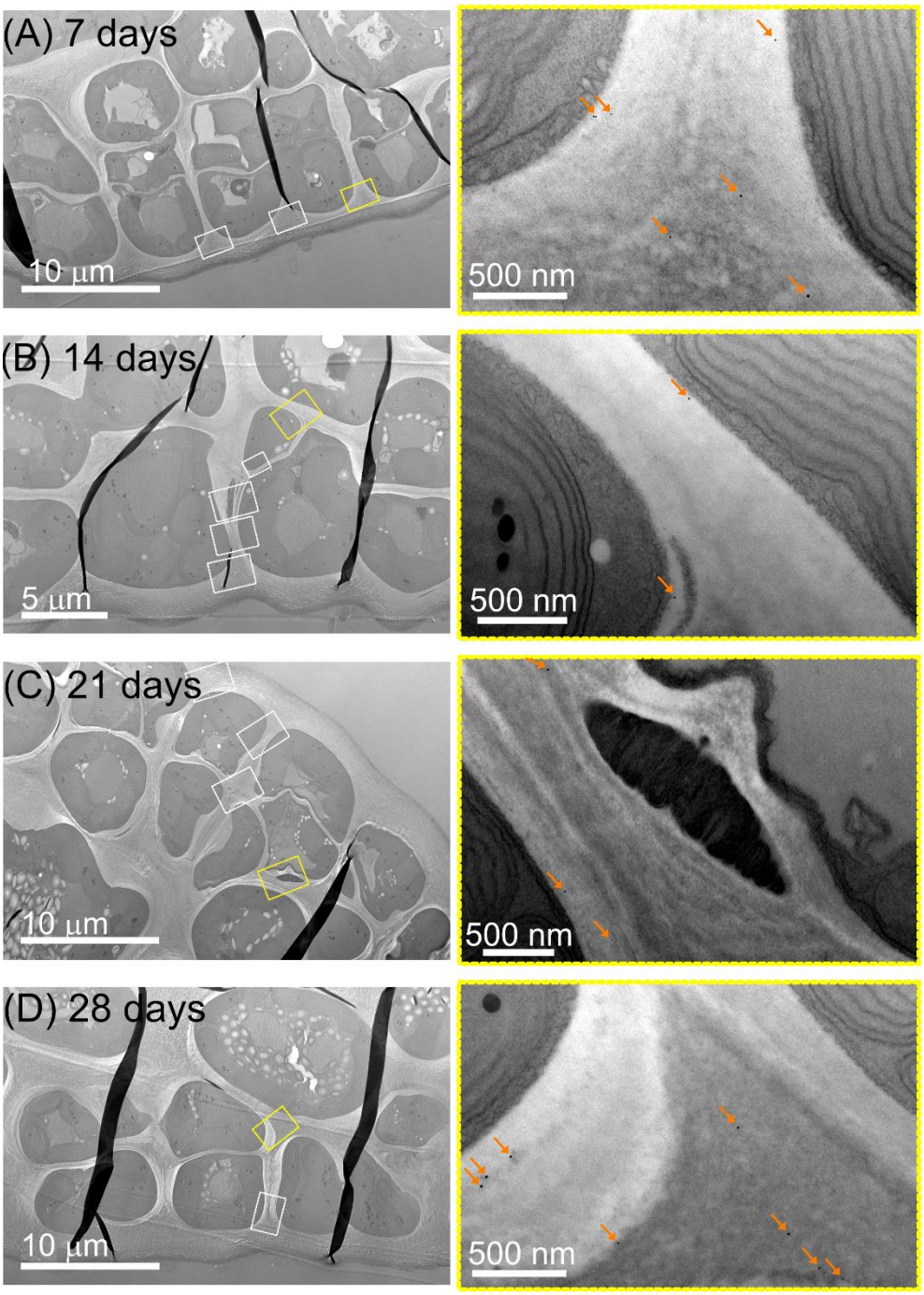

Figure 4. Biodistribution of PVP-AgNPs in *P. palmata* after (A) 7, (B) 14, (C) 21, and (D) 28 days of exposure. The different squares in the lower magnification TEM images (left) indicate the tissue's positions analysed at higher magnification. TEM images acquired in the area framed by yellow squares are shown on the right panel, which shows the deepest localised AgNPs in the tissue at each time point. The rest of the TEM images acquired at higher magnification into the area framed by white squares can be found in the supporting information: Figure S16 for 7 days of exposure; Figure S19 for 14 days of exposure; Figure S21 for 21 days of exposure, and Figure S23 for 28 days of exposure. The orange arrows indicate the position of the localised AgNPs.

To better understand the biodistribution and the possible chemical transformation of internalised PVP-AgNPs, we analysed several tissue sections of both seaweeds at different exposure times by TEM and STEM-EDX. **Figure 3** shows TEM images of *U. fenestrata* exposed to PVP-AgNPs after 7, 14, 21, and 28 days of exposure. The distribution of AgNPs was similar at all exposure times. The NPs penetrated the cuticle, mucilage and intercellular space, and cell wall at early stages (i.e., 7 days, see **Figure 3A**, **Figure S7,** and **Figure S8**) and advanced in the tissue by moving between cells via the inner cell wall. The AgNPs' fate had the same tendency in the other three time points as observed in **Figure 3B**, **Figure S9**, **S10**, and **S11** for 14 days, **Figure 3C**, **Figure S12**, and **S13** for 21 days, and **Figure 3D** and **Figure S14** for 28 days. We observed a concentration gradient in the AgNPs distribution from the highest number of NPs next to the cell walls of the cortical cells (e.g., see **Figure S6**, **S9**, **S12,** and **S14**) to the lowest number of NPs in the deepest localisation of the tissue (see TEM images highlighted yellow square with high magnification in **Figure 3**). We also measured the NP size inside *U. fenestrata* (**Figure S15**), demonstrating that AgNPs became smaller, 19 – 12 nm in diameter, than the initial primary size in RSW, ~25 nm in diameter, (**Figure 1A**) and after 7 days of incubation in RSW, ~26 nm (**Figure 1B**). This feature indicated that AgNPs underwent a higher percentage of dissolution when they were internalised in the tissue than when they were incubated in RSW (**Figure 1A** and **B** and **Figure S3**).

In contrast to the results from *U. fenestrata*, the biodistribution of PVP-AgNPs in *P. palmata* showed a different behaviour. After 7 days of exposure, all particles in *P. palmata* were confined between the cuticle and the mucilage with some exceptions since some NPs could be localised close to the first line of cortical cells as shown in **Figure 4A**, **S16**, **S17,** and **S18**. **Figure S17A** confirmed the absence of NPs in deeper localisations (i.e., in the intracellular space and cell wall) at this time point. At 14 days, NPs were already channelled through the intercellular space, reaching a deeper location in the tissue (see **Figure 4B**, **S19,** and **S20**). Also, in some cases, a possible cellular internalisation could be suggested (see TEM images highlighted with a cyan square in **Figure S19**). We observed similar behaviour in the NP distribution after 21 (**Figure 4C**, **S21,** and **S22**) and 28 days (**Figure 4D** and **S23**) of exposure when the particles tended to accumulate all along the cell wall close to the cell membrane

and did not pass the second line of cells that belongs to the cortex. The number of NPs accumulated increased as a function of exposure time: from < 10 NPs counted after 7 days in any of the tissue sections analysed to > 15 NPs found both after 21 and 28 days (see TEM images included in SI). Moreover, as in the case of *U. fenestrata*, the NPs size also decreased inside of *P. palmata* with respect to the size of these NPs incubated in RSW: 15 – 22 nm internalised AgNPs (**Figure S15**) *vs* 26 nm AgNPs (**Figure 1B**), confirming that higher percentage of dissolution occurred during the internalisation.

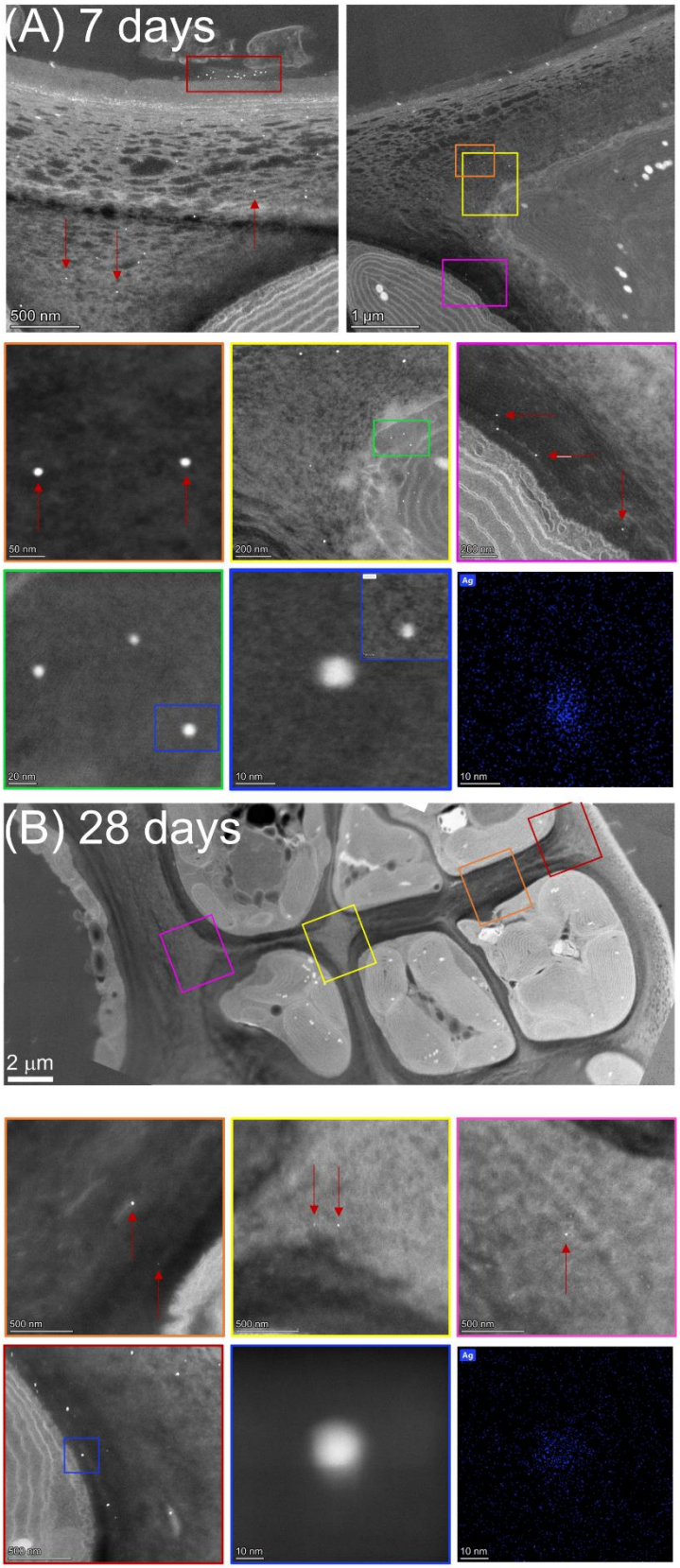

Figure 5. Distribution of PVP-AgNPs in *P. palmata* after 7 (A) and 28 (B) days of exposure. From the top, high angle annular dark field (HAADF) low magnification images of cells organisation. High magnification images where AgNPs (bright dots) are pointed by red arrows and squared. At the bottom, STEM-EDX elemental mapping of the area of interest, confirming the presence of Ag. **Figure S24** shows the relative mass percentages

of the elements detected when EDX maps were analyaed in both areas and in the presence and absence (i.e., only tissue) of AgNP.

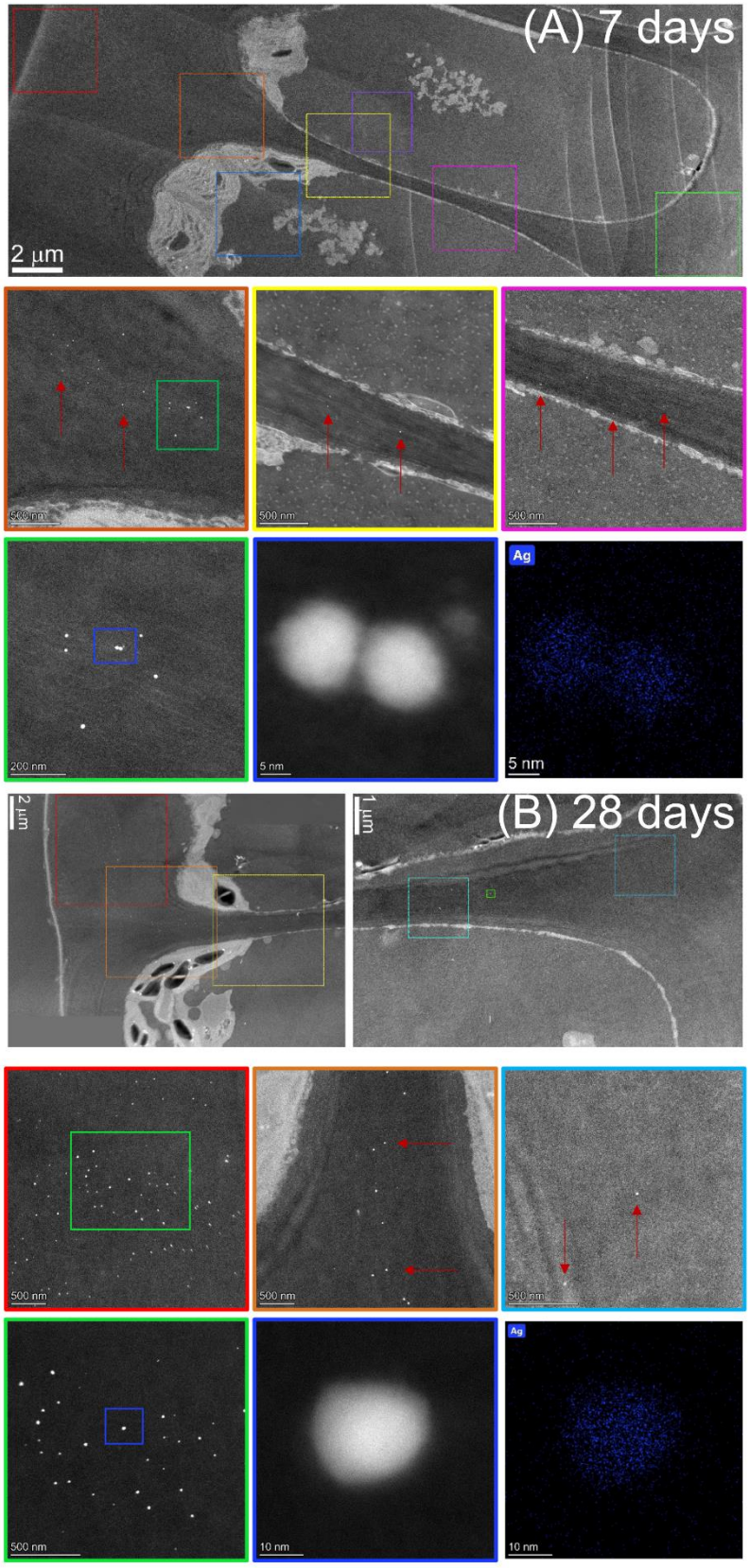

Figure 6. Distribution of PVP-AgNPs in *U. fenestrata* after 7 (A) and 28 (B) days of exposure. From the top, high angle annular dark field (HAADF) low magnification images of cells organisation. High magnification

images where AgNPs (bright dots) are pointed by red arrows and squared. At the bottom, STEM-EDX elemental mapping of the area of interest, confirming the presence of Ag. **Figure S25** shows the relative mass percentages of the elements detected when EDX maps were analysed in both areas and in the presence and absence (i.e., only tissue) of AgNP.

We also investigated the biodistribution using STEM integrated with an energy dispersive X-ray (EDX) detector to study the chemical transformation of PVP-AgNPs after internalisation. STEM images confirmed the same particle's fate observed by TEM: at 7 days of exposure, *P. palmata* found a significant part of the NPs to accumulate outside the cuticle and many in the mucilage and polysaccharides intercellular matrix right before the beginning of the first line of cells, with some NPs even inside the chloroplasts, thus, having trespassed the cell membrane (**Figure 5**); while in *U. fenestrata*, no NPs were found close to the cell membrane, but were instead localised in the intercellular matrix and cell walls (**Figure 6**). No NPs were observed in the cell cytoplasm or organelles in this condition. In both seaweeds, going through the different time points, it was possible to follow the particles gradually reaching the inner areas of the tissue. EDX mapping identified the silver element in the spherical electron-dense NPs with a diameter between 8 – 20 nm, confirming the bioaccumulation of AgNPs. We found several electron-dense NPs with different shapes and sizes that were identified as other inorganic nanoparticles (**Figure S27**), demonstrating the importance of the chemical identification of the electron-dense particles visualised in the tissue.

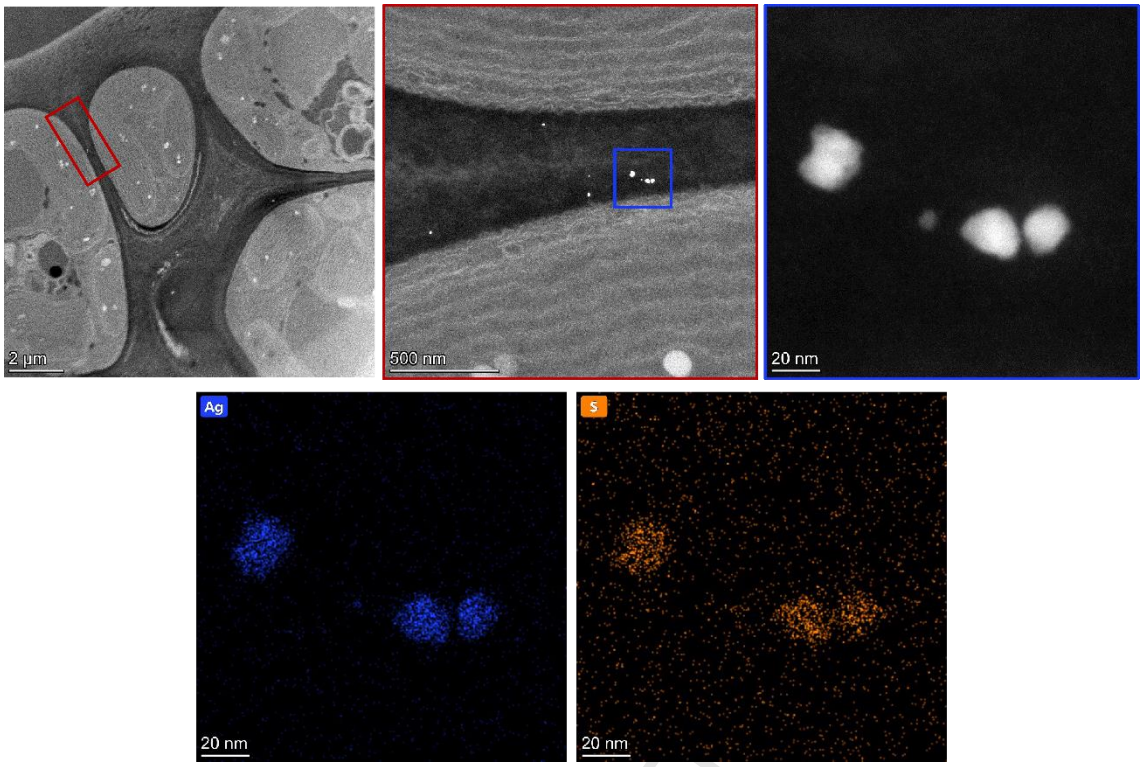

Figure 7. Representative STEM-EDX images showing the particle's transformation processes in *P. palmata* after 21 days of exposure. The co-localisation of Ag (blue) and S (orange) in the EDX maps provides evidence about the formation of sulfur-rich corona or/and sulfidation undergone by AgNPs. **Figure S26** shows the relative mass percentages of the elements detected when EDX maps were analysed in both areas and in the presence and absence (i.e., only tissue) of AgNP.

Considering the decrease in size of AgNPs during the internalisation into tissues and their possible interactions with the matrix, we decided to investigate the potential transformation of AgNPs that occurs within the seaweed's tissues since the chemical speciation of the NPs could modify the potential risk associated with their accumulation. STEM-EDX analysis of the tissues was performed at different times of exposure and in areas where only tissue and AgNPs were observed. The possible transformations of AgNPs are oxidative dissolution, formation of sulfur-rich corona or/and sulfidation, and chlorination (Zhang et al., 2018). Therefore, we investigated the peaks related to O, S, and Cl that may be identified together with Ag in the EDX spectra acquired in the area occupied by AgNPs. Only a relationship between S and Ag was clearly identified in all the cases (**Figure S24**, **S25**, **S26**, and **S28**). Chlorine was only detected in a few cases and no correlation could be established. The presence of chlorine could come from the adsorption of this element on the Ag surface from seawater. Although silver and sulfur were also detected in the area that only contained

tissue, the relative mass percentages were lower, 10 – 100 times for Ag and 3 – 9 times for S, than in the area occupied by AgNP (**Figure S24**, **S25**, and **S26**). It is well-known that seaweeds contain sulfur-rich proteins and polysaccharides, and they synthesise and store more sulfur-containing compounds than terrestrial plants (Mensi et al., 2022). Therefore, it is reasonable to think that the main transformation of PVP-AgNPs could be the formation of sulfur-rich corona and/or sulfidation. Stegemeier et al. had already observed that the main transformation of AgNPs internalised by the aquatic plant *Landoltia punctata* (Duckweed) was sulfidation. However, the tissue biodistribution of those NPs was not assessed (Stegemeier et al., 2017). Moreover, the formation of sulfur-rich corona around AgNPs cannot be discarded due to the potential rapid exchange of PVP by macromolecules present in the seaweed composition. It has been reported that this coating formed around Ag surface could trap released silver ions by forming silver sulphide on the NP surface (Miclăuş et al., 2016). **Figure 7** shows an example of the procedure followed in this study. We localised the AgNPs inside the seaweed tissue by STEM and then acquired EDX maps and mass percentages from Ag and S in 3 to 7 NPs per time of exposure. By following the Ag/S ratio associated with the particles located in different regions of the tissue, we then assessed the degree of transformation related to the formation of sulfur-rich corona and/or sulfidation as a function of tissue penetration and exposure time. **Figure 8A** shows that *U. fenestrata* presented AgNPs with an almost stable Ag/S ratio over all exposure times, while *P. palmata*, showed a decrease in sulfur content on AgNP with longer exposure times. Interestingly, the sulfur-rich corona/sulfidation after 28 days of exposure in *P. palmata* presented higher heterogeneity. We analysed the localisation of each AgNPs in the STEM image and we observed that the lowest sulfur content was found in the AgNPs closer to the seaweed surface as shown in **Figure 8B**, pointing out a transformation that advances with time and/or level of penetration in the tissue. The heterogeneity of the sulfur-rich corona/sulfidation observed in *P. palmata*, more evident after 28 days of exposure, could also be explained by an increase in the size of the single AgNPs inside the seaweed due to the regeneration of internalised AgNPs for the reduction of the dissolved ionic Ag onto these available NPs, which act as nucleation points (Zou et al., 2017): the higher the size of the NP, the lowest the ratio of sulfur as the available surface decreases. **Figure S29** shows the size of AgNPs internalised by *P. palmata* analysed by EDX after 28 days of exposure (see

Figure 8) estimated using HRTEM images, demonstrating that the highest Ag/S ratio, i.e., lowest sulfur content, calculated for AgNP closer to the seaweed surface is correlated with the higher size displayed for this NP: 15 nm for AgNP in *(1)* versus 13 nm for AgNPs in *(2)* and *(3)*. Sulphate groups' level in cellulose nanocrystals has been reported to have a critical role in the growth, size distribution, and stability of AgNPs synthesised in its presence (Lokanathan et al., 2014). Sulphated polysaccharides (SPs) have the potential to reduce silver ions and cap AgNPs. Higher AgNPs average size was found in the last time points of *P. palmata* exposure, as shown in **Figure S15**, while the size distribution of the population is kept quite homogeneous (SD ≤ 6 nm), which seems more consistent with an increase in the size of the initial AgNPs inside the seaweed. In addition, ICP-MS results showed a higher discrepancy between the total ionic silver and the number of NPs/g estimated in *P. palmata* (**Figure 2** and **Figure S6**), which may demonstrate the higher availability of ionic silver to regenerate NPs. Although *de novo* synthesis cannot be ruled out, Jeon et al. reported the rapid synthesis of AgNPs with an average size of 24 nm using SPs extracted from the marine Rhodophyta, *Porphyridium cruentum* (Jeon et al., 2021). SP is an acidic heteropolymer composed of D-xylose, D-glucose, D-, and L-galactose. It contains approximately 10% sulphate ester. However, if a good part of the dissolved Ag would form new NPs, a broader size distribution would be expected, unlike the initial AgNPs.

Despite this clear internalisation and transport across the tissue, scarce cell membrane transport was verified; the sulphate groups in the AgNPs surface could be responsible for a lower cell uptake or diffusion, as the sulphated polysaccharides would confer electronegative charge and, consequently, electrostatic repulsion with the cell membrane, can occur (Jeon et al., 2021).

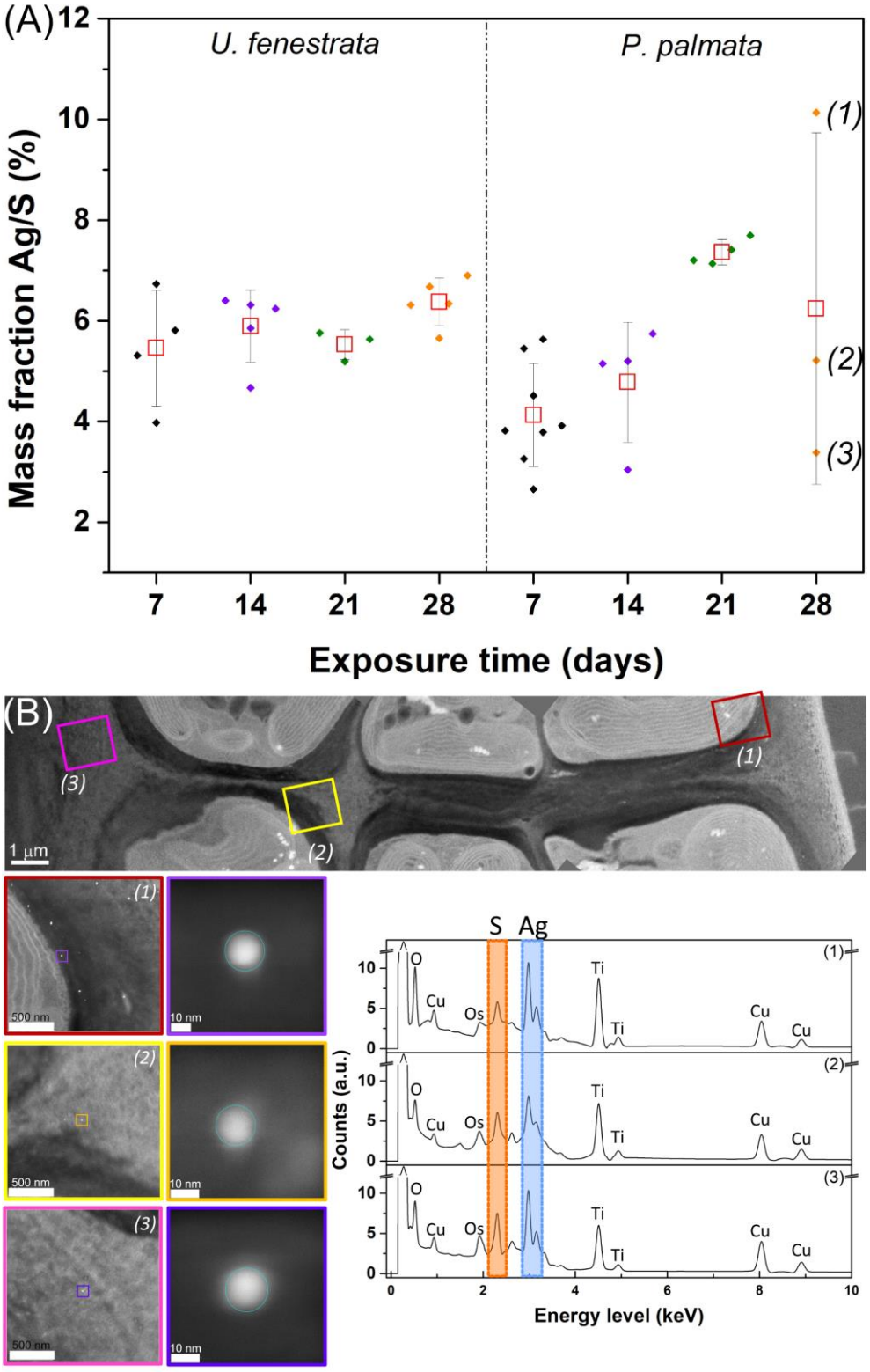

Figure 8. (A) Mass fraction percentage of Ag/S ratio estimated at different times of exposure in *U. fenestrata* and *P. palmata*, respectively. The highest variability in the Ag/S mass fraction was observed in *P. palmata* after 28 days of exposure. To understand this, (B) shows a low-magnification STEM image, which shows the localisation of AgNPs within the tissue. This image was processed by merging 3 individual STEM images at the same magnification using Affinity Photo (version 1.10.5.1342). STEM images at higher magnification indicate the position where the EDX maps were acquired. The cyan circular frames indicate the area analysed, where the

AgNPs were localised, whose spectra are reported. The atomic and mass percentages of elements detected in EDX maps are shown in **Figure S27**. Both in (A) and in (B), analysed AgNPs are labelled by (1), (2), and (3), respectively. The size estimated by HRTEM images of these AgNPs is included in **Figure S29**.

The explanation of the difference in the biodistribution and transformation level that the particles were subjected to could also be found in the different cell wall compositions that the two seaweed species presented. In the case of *U. fenestrata*, the cell walls are mainly composed of cellulose, xyloglucan, and ulvan. We paid attention to ulvan, which is mainly composed of repeating units of sulphated disaccharides involving β-d-glucuronic acid (1 → 4)-α-1-rhamnose-3-sulfate, and α-l-iduronic acid (1 → 4)-α-l-rhamnose-3-sulfate (Wahlström et al., 2020). At the same time, the main component of the cell walls in *P. palmata* is β-(1 → 4)- and β-(1 → 3)-linked D-xylose units in a proportion of about 4:1 (Stévant et al., 2023). Interestingly, hydrogen bounds hold these partly acidic units in the cell wall (Deniaud et al., 2003). In addition, this acidity of the xylans is produced by a covalent link with sulphated and/or phosphorylated xylogalactoprotein complex (Wang et al., 2020). This could allow hypothesising about the difference in the AgNPs transportation and their sulfur-rich corona formation and/or sulfidation between both seaweeds. These hydrogen bonds may produce a more compact and rigid cross-linked polysaccharide, which would hinder the NPs' transportation through the cell wall of *P. palmata*. Therefore, we could also explain that the biodistribution of AgNPs in *P. palmata* was time-dependent; while in *U. fenestrata* the distribution was homogeneous at all exposure times studied (**Figure 3** for *U. fenestrata* and **Figure 4** for *P. palmata*).

We could also attribute the variation of sulfur-rich corona formation/sulfidation of AgNPs to the difference in the cell wall composition. Water-soluble sulphated polysaccharide ulvan in green seaweed is homogeneously distributed in the cell wall, allowing "easier" interactions of the sulphate groups with Ag surface, and then the complexation Ag-SO_3-R should be favoured (Levard et al., 2012). In the case of red seaweed, the sulphated xylogalactoproteins are linked to the xylans, which should affect the complexation Ag-SO_3-R. It is worth noting that other sulfur-rich biomolecules, such as S-containing proteins present in the cell wall, may contribute to the AgNP's transformation (Grill et al., 1987). Also, phytochelatins produced during the depuration mechanism could play an important role in AgNPs transformation because they are 5-17-aminoacids-length peptides of repetitive γ-

glutamylcysteine units with carboxyl-terminal glycine. These γ-glutamylcysteine units can interact with the Ag surface, forming Ag_2S-like complexes (Toh et al., 2014).

Conclusions

In summary, we reported for the first time, to the best of our knowledge, the biodistribution of bioaccumulated PVP-AgNPs and the transformation they undergo into two seaweeds: *P. palmata* and *U. fenestrata*. Some questions remain open and should be explored in subsequent studies. One of them is to elucidate the oxidation state of both Ag and S observed in the EDX analysis, which would allow us to understand the complex compound formed and thus to be able to better predict the potential response of the seaweed against exposure to these NPs. Sulfidation significantly decreases the solubility and availability of Ag ions and consequently, their toxicity. However, because of the potential accumulation and long-term stability of Ag_2S-NPs in the environment, it is necessary to evaluate chronic exposure effects. Additionally, it is essential to consider that sulphate groups do not avoid dissolution of Ag as efficiently as sulphide (López-Mayán et al., 2022).

Follow-up studies are being conducted on the bioaccessibility and bioavailability of the AgNPs accumulated in seaweed through the human gastrointestinal tract. Altogether, these works will help to better evaluate the human risk of exposure to accumulated AgNPs by oral intake of commercial seaweed, which is increasingly explored and used as an alternative and nutritive food source.

Acknowledgments

The authors acknowledge funding from NANOCULTURE Interreg Atlantic Area project (EAPA_590/2018) and SbDToolBox- Nanotechnology-based tools and tests for Safe-by-Design nanomaterials (NORTE-01-0145-FEDER-000047) supported by North Portugal Regional Operational Programme (NORTE2020) under the PORTUGAL 2020 Partnership Agreement through the European

Regional Development Fund (ERDF). L.R.-L. acknowledges funding to FCT (Fundação para a Ciência e Technologia) for the Scientific Employment Stimulus Program (2020.04021.CEECIND).

We thank the Nanophotonics & Bioimaging and AEMIS facilities and staff at INL and Centre for Scientific and Technological Support to Research (CACTI) at University of Vigo for their contribution.

Author contributions

L.R.-L. and B.E. designed the project. M.Q. performed the preparation of AgNPs, their characterisation and STEM-EDX analysis. I.P. carried out the sample preparation for EM. M.M. performed the bioaccumulation assays. J.J.L.-M. and A.M.-P. performed and analysed the ICP-MS and spICP-MS. M.S.-C. acquired the TEM images and prepared the 3D images in Figure 1. L.R.-L. acquired and analysed the TEM images. The manuscript was written through the contributions of all authors. All authors have given approval to the final version of the manuscript.

Ethics declaration

Competing interest

The authors declare no competing interest.

Data availability

Upon the manuscript's acceptance, all raw data used to prepare the figures and tables included in it and supporting information will be uploaded to Zenodo.

References

Araújo, R., Vázquez Calderón, F., Sánchez López, J., Azevedo, I.C., Bruhn, A., Fluch, S., Garcia Tasende, M., Ghaderiardakani, F., Ilmjärv, T., Laurans, M., Mac Monagail, M., Mangini, S., Peteiro, C., Rebours, C., Stefansson, T., Ullmann, J., 2021. Current Status of the Algae Production Industry in Europe: An Emerging Sector of the Blue Bioeconomy. Front Mar Sci 7. https://doi.org/10.3389/fmars.2020.626389

Blinova, I., Niskanen, J., Kajankari, P., Kanarbik, L., Käkinen, A., Tenhu, H., Penttinen, O.-P., Kahru, A., 2013. Toxicity of two types of silver nanoparticles to aquatic crustaceans Daphnia magna and Thamnocephalus platyurus. Environmental Science and Pollution Research 20, 3456–3463. https://doi.org/10.1007/s11356-012-1290-5

Bouga, M., Combet, E., 2015. Emergence of Seaweed and Seaweed-Containing Foods in the UK: Focus on Labeling, Iodine Content, Toxicity and Nutrition. Foods 4, 240–253. https://doi.org/10.3390/foods4020240

Calisi, A., Lorusso, C., Gallego-Urrea, J.A., Hassellöv, M., Dondero, F., 2022. Ecotoxicological effects of silver nanoparticles in marine mussels. Science of The Total Environment 851, 158113. https://doi.org/10.1016/j.scitotenv.2022.158113

Cervantes-Avilés, P., Huang, Y., Keller, A.A., 2019. Multi-technique approach to study the stability of silver nanoparticles at predicted environmental concentrations in wastewater. Water Res 166, 115072. https://doi.org/10.1016/j.watres.2019.115072

Chernousova, S., Epple, M., 2013. Silver as Antibacterial Agent: Ion, Nanoparticle, and Metal. Angewandte Chemie International Edition 52, 1636–1653. https://doi.org/10.1002/anie.201205923

Cvjetko, P., Zovko, M., Štefanić, P.P., Biba, R., Tkalec, M., Domijan, A.-M., Vrček, I.V., Letofsky-Papst, I., Šikić, S., Balen, B., 2018. Phytotoxic effects of silver nanoparticles in tobacco plants. Environmental Science and Pollution Research 25, 5590–5602. https://doi.org/10.1007/s11356-017-0928-8

Deniaud, E., Quemener, B., Fleurence, J., Lahaye, M., 2003. Structural studies of the mix-linked β-(1→3)/β-(1→4)-d-xylans from the cell wall of Palmaria palmata (Rhodophyta). Int J Biol Macromol 33, 9–18. https://doi.org/10.1016/S0141-8130(03)00058-8

Dhargalkar, V.K., Verlecar, X.N., 2009. Southern Ocean seaweeds: A resource for exploration in food and drugs. Aquaculture 287, 229–242. https://doi.org/10.1016/j.aquaculture.2008.11.013

García-Alonso, J., Khan, F.R., Misra, S.K., Turmaine, M., Smith, B.D., Rainbow, P.S., Luoma, S.N., Valsami-Jones, E., 2011. Cellular Internalization of Silver Nanoparticles in Gut Epithelia of the Estuarine Polychaete *Nereis diversicolor*. Environ Sci Technol 45, 4630–4636. https://doi.org/10.1021/es2005122

Giusti, L., 2001. Heavy metal contamination of brown seaweed and sediments from the UK coastline between the Wear river and the Tees river. Environ Int 26, 275–286. https://doi.org/10.1016/S0160-4120(00)00117-3

Gökçe, D., 2016. Algae as an Indicator of Water Quality, in: Algae - Organisms for Imminent Biotechnology. InTech. https://doi.org/10.5772/62916

Gonçalves, J.M., Bebianno, M.J., 2023. Ecotoxicity of emerging contaminants in the reproductive organ of marine mussels Mytilus galloprovincialis. Science of The Total Environment 881, 163486. https://doi.org/10.1016/j.scitotenv.2023.163486

Grill, E., Winnacker, E.-L., Zenk, M.H., 1987. Phytochelatins, a class of heavy-metal-binding peptides from plants, are functionally analogous to metallothioneins. Proceedings of the National Academy of Sciences 84, 439–443. https://doi.org/10.1073/pnas.84.2.439

Huang, D., Dang, F., Huang, Y., Chen, N., Zhou, D., 2022. Uptake, translocation, and transformation of silver nanoparticles in plants. Environ Sci Nano 9, 12–39. https://doi.org/10.1039/D1EN00870F

Jang, M.-H., Kim, W.-K., Lee, S.-K., Henry, T.B., Park, J.-W., 2014. Uptake, Tissue Distribution, and Depuration of Total Silver in Common Carp (*Cyprinus carpio*) after Aqueous Exposure to Silver Nanoparticles. Environ Sci Technol 48, 11568–11574. https://doi.org/10.1021/es5022813

Jeon, M.S., Han, S.-I., Park, Y.H., Kim, H.S., Choi, Y.-E., 2021. Rapid green synthesis of silver nanoparticles using sulfated polysaccharides originating from Porphyridium cruentum UTEX 161: evaluation of antibacterial and catalytic activities. J Appl Phycol 33, 3091–3101. https://doi.org/10.1007/s10811-021-02540-x

Jönsson, M., Nordberg Karlsson, E., 2024. Chemical food safety of seaweed: Species, spatial and thallus dependent variation of potentially toxic elements (PTEs) and techniques for their removal. J Appl Phycol 36, 765–781. https://doi.org/10.1007/s10811-023-03131-8

Jorge de Souza, T.A., Rosa Souza, L.R., Franchi, L.P., 2019. Silver nanoparticles: An integrated view of green synthesis methods, transformation in the environment, and toxicity. Ecotoxicol Environ Saf 171, 691–700. https://doi.org/10.1016/j.ecoenv.2018.12.095

Kim, Y.S., Song, M.Y., Park, J.D., Song, K.S., Ryu, H.R., Chung, Y.H., Chang, H.K., Lee, J.H., Oh, K.H., Kelman, B.J., Hwang, I.K., Yu, I.J., 2010. Subchronic oral toxicity of silver nanoparticles. Part Fibre Toxicol 7, 20. https://doi.org/10.1186/1743-8977-7-20

Kose, O., Mantecca, P., Costa, A., Carrière, M., 2023. Putative adverse outcome pathways for silver nanoparticle toxicity on mammalian male reproductive system: a literature review. Part Fibre Toxicol 20, 1. https://doi.org/10.1186/s12989-022-00511-9

Kyrychenko, A., Korsun, O.M., Gubin, I.I., Kovalenko, S.M., Kalugin, O.N., 2015. Atomistic Simulations of Coating of Silver Nanoparticles with Poly(vinylpyrrolidone) Oligomers: Effect of Oligomer Chain Length. The Journal of Physical Chemistry C 119, 7888–7899. https://doi.org/10.1021/jp510369a

Levard, C., Hotze, E.M., Lowry, G. V., Brown, G.E., 2012. Environmental Transformations of Silver Nanoparticles: Impact on Stability and Toxicity. Environ Sci Technol 46, 6900–6914. https://doi.org/10.1021/es2037405

Li, L., Stoiber, M., Wimmer, A., Xu, Z., Lindenblatt, C., Helmreich, B., Schuster, M., 2016. To What Extent Can Full-Scale Wastewater Treatment Plant Effluent Influence the Occurrence of Silver-Based Nanoparticles in Surface Waters? Environ Sci Technol 50, 6327–6333. https://doi.org/10.1021/acs.est.6b00694

Li, Y., Cummins, E., 2021. A semi-quantitative risk ranking of potential human exposure to engineered nanoparticles (ENPs) in Europe. Science of The Total Environment 778, 146232. https://doi.org/10.1016/j.scitotenv.2021.146232

Liu, H., Wang, Xinxin, Wu, Y., Hou, J., Zhang, S., Zhou, N., Wang, Xiangke, 2019. Toxicity responses of different organs of zebrafish (Danio rerio) to silver nanoparticles with different particle sizes and surface coatings. Environmental Pollution 246, 414–422. https://doi.org/10.1016/j.envpol.2018.12.034

Lokanathan, A.R., Uddin, K.M.A., Rojas, O.J., Laine, J., 2014. Cellulose Nanocrystal-Mediated Synthesis of Silver Nanoparticles: Role of Sulfate Groups in Nucleation Phenomena. Biomacromolecules 15, 373–379. https://doi.org/10.1021/bm401613h

López-Mayán, J.J., Álvarez-Fernández, B., Peña-Vázquez, E., Barciela-Alonso, M.C., Moreda-Piñeiro, A., Bermejo-Barrera, P., 2022. Ultrasonication followed by enzymatic hydrolysis as a sample pre-treatment for the determination of Ag nanoparticles in edible seaweed by SP-ICP-MS. Talanta 247, 123556. https://doi.org/10.1016/j.talanta.2022.123556

López-Mayán, J.J., Álvarez-Fernández, B., Peña-Vázquez, E., Barciela-Alonso, M.C., Moreda-Piñeiro, A., Maguire, J., Mackey, M., Quarato, M., Pinheiro, I., Espiña, B., Rodríguez-Lorenzo, L., Bermejo-Barrera, P., 2023. Bioaccumulation of titanium dioxide nanoparticles in green (Ulva sp.) and red (Palmaria palmata) seaweed. Microchimica Acta 190, 287. https://doi.org/10.1007/s00604-023-05849-1

Mat Lazim, Z., Salmiati, S., Marpongahtun, M., Arman, N.Z., Mohd Haniffah, M.R., Azman, S., Yong, E.L., Salim, M.R., 2023. Distribution of Silver (Ag) and Silver Nanoparticles (AgNPs) in Aquatic Environment. Water (Basel) 15, 1349. https://doi.org/10.3390/w15071349

Meng, J., Ji, Y., Liu, J., Cheng, X., Guo, H., Zhang, W., Wu, X., Xu, H., 2014. Using gold nanorods core/silver shell nanostructures as model material to probe biodistribution and toxic effects of silver nanoparticles in mice. Nanotoxicology 8, 686–696. https://doi.org/10.3109/17435390.2013.822593

Mensi, F., Ben Ghedifa, A., Rajhi, H., 2022. Effects of seawater sulfur starvation and enrichment on Gracilaria gracilis growth and biochemical composition. Sci Rep 12, 11095. https://doi.org/10.1038/s41598-022-15303-6

Miclăuș, T., Beer, C., Chevallier, J., Scavenius, C., Bochenkov, V.E., Enghild, J.J., Sutherland, D.S., 2016. Dynamic protein coronas revealed as a modulator of silver nanoparticle sulphidation in vitro. Nat Commun 7, 11770. https://doi.org/10.1038/ncomms11770

Moore, T.L., Rodriguez-Lorenzo, L., Hirsch, V., Balog, S., Urban, D., Jud, C., Rothen-Rutishauser, B., Lattuada, M., Petri-Fink, A., 2015. Nanoparticle colloidal stability in cell culture media and impact on cellular interactions. Chem Soc Rev 44, 6287–6305. https://doi.org/10.1039/C4CS00487F

Nabi, M.M., Wang, J., Meyer, M., Croteau, M.-N., Ismail, N., Baalousha, M., 2021. Concentrations and size distribution of TiO2 and Ag engineered particles in five wastewater treatment plants in the United States. Science of The Total Environment 753, 142017. https://doi.org/10.1016/j.scitotenv.2020.142017

Niu, Z., Xu, M., Guo, X., Yan, J., Liu, M., Yang, Y., 2023. Uptake of Silver-Containing Nanoparticles in an Estuarine Plant: Speciation and Bioaccumulation. Environ Sci Technol 57, 16075–16085. https://doi.org/10.1021/acs.est.3c04774

Parodi, A., Leip, A., De Boer, I.J.M., Slegers, P.M., Ziegler, F., Temme, E.H.M., Herrero, M., Tuomisto, H., Valin, H., Van Middelaar, C.E., Van Loon, J.J.A., Van Zanten, H.H.E., 2018. The potential of future foods for sustainable and healthy diets. Nat Sustain 1, 782–789. https://doi.org/10.1038/s41893-018-0189-7

Peng, Z., Guo, Z., Wang, Z., Zhang, R., Wu, Q., Gao, H., Wang, Y., Shen, Z., Lek, S., Xiao, J., 2022. Species-specific bioaccumulation and health risk assessment of heavy metal in seaweeds in tropic coasts of South China Sea. Science of The Total Environment 832, 155031. https://doi.org/10.1016/j.scitotenv.2022.155031

Plascencia-Villa, G., Ponce, A., Collingwood, J.F., Arellano-Jiménez, M.J., Zhu, X., Rogers, J.T., Betancourt, I., José-Yacamán, M., Perry, G., 2016. High-resolution analytical imaging and electron holography of magnetite particles in amyloid cores of Alzheimer's disease. Sci Rep 6, 24873. https://doi.org/10.1038/srep24873

Qi, M., Wang, X., Chen, J., Liu, Yin, Liu, Yun, Jia, J., Li, L., Yue, T., Gao, L., Yan, B., Zhao, B., Xu, M., 2023. Transformation, Absorption and Toxicological Mechanisms of Silver Nanoparticles in the Gastrointestinal Tract Following Oral Exposure. ACS Nano 17, 8851–8865. https://doi.org/10.1021/acsnano.3c00024

Quarato, M., Pinheiro, I., Vieira, A., Espiña, B., Rodriguez-Lorenzo, L., 2021. Detection of Silver Nanoparticles in Seawater Using Surface-Enhanced Raman Scattering. Nanomaterials 11, 1711. https://doi.org/10.3390/nano11071711

Sadri, S., Khoei, A.J., 2023. Ambient salinity affects silver nanoparticles (AgNPs) induced toxicity in the marine bivalve, the rock oyster, Saccostrea cucullata. Aquac Rep 30, 101596. https://doi.org/10.1016/j.aqrep.2023.101596

Scimeca, M., Bischetti, S., Lamsira, H.K., Bonfiglio, R., Bonanno, E., 2018. Energy Dispersive X-ray (EDX) microanalysis: A powerful tool in biomedical research and diagnosis. European Journal of Histochemistry. https://doi.org/10.4081/ejh.2018.2841

Seregin, I. V., Kozhevnikova, A.D., 2023. Phytochelatins: Sulfur-Containing Metal(loid)-Chelating Ligands in Plants. Int J Mol Sci 24, 2430. https://doi.org/10.3390/ijms24032430

Sikder, M., Lead, J.R., Chandler, G.T., Baalousha, M., 2018. A rapid approach for measuring silver nanoparticle concentration and dissolution in seawater by UV–Vis. Science of The Total Environment 618, 597–607. https://doi.org/10.1016/j.scitotenv.2017.04.055

Stegemeier, J.P., Colman, B.P., Schwab, F., Wiesner, M.R., Lowry, G. V., 2017. Uptake and Distribution of Silver in the Aquatic Plant *Landoltia punctata* (Duckweed) Exposed to Silver and Silver Sulfide Nanoparticles. Environ Sci Technol 51, 4936–4943. https://doi.org/10.1021/acs.est.6b06491

Stegemeier, J.P., Schwab, F., Colman, B.P., Webb, S.M., Newville, M., Lanzirotti, A., Winkler, C., Wiesner, M.R., Lowry, G. V., 2015. Speciation Matters: Bioavailability of Silver and Silver Sulfide Nanoparticles to Alfalfa (*Medicago sativa*). Environ Sci Technol 49, 8451–8460. https://doi.org/10.1021/acs.est.5b01147

Steinhagen, S., Enge, S., Larsson, K., Olsson, J., Nylund, G.M., Albers, E., Pavia, H., Undeland, I., Toth, G.B., 2021. Sustainable Large-Scale Aquaculture of the Northern Hemisphere Sea Lettuce, Ulva fenestrata, in an Off-Shore Seafarm. J Mar Sci Eng 9, 615. https://doi.org/10.3390/jmse9060615

Stévant, P., Schmedes, P.S., Le Gall, L., Wegeberg, S., Dumay, J., Rebours, C., 2023. Concise review of the red macroalga dulse, Palmaria palmata (L.) Weber & Mohr. J Appl Phycol 35, 523–550. https://doi.org/10.1007/s10811-022-02899-5

Tejamaya, M., Römer, I., Merrifield, R.C., Lead, J.R., 2012. Stability of Citrate, PVP, and PEG Coated Silver Nanoparticles in Ecotoxicology Media. Environ Sci Technol 46, 7011–7017. https://doi.org/10.1021/es2038596

Toh, H.S., Batchelor-McAuley, C., Tschulik, K., Compton, R.G., 2014. Chemical interactions between silver nanoparticles and thiols: a comparison of mercaptohexanol against cysteine. Sci China Chem 57, 1199–1210. https://doi.org/10.1007/s11426-014-5141-8

Turner, A., Brice, D., Brown, M.T., 2012. Interactions of silver nanoparticles with the marine macroalga, Ulva lactuca. Ecotoxicology 21, 148–154. https://doi.org/10.1007/s10646-011-0774-2

Wahlström, N., Nylander, F., Malmhäll-Bah, E., Sjövold, K., Edlund, U., Westman, G., Albers, E., 2020. Composition and structure of cell wall ulvans recovered from Ulva spp. along the Swedish west coast. Carbohydr Polym 233, 115852. https://doi.org/10.1016/j.carbpol.2020.115852

Wang, Y.-C., Chen, Y.-C., Chuang, W.-S., Li, J.-H., Wang, Y.-S., Chuang, C.-H., Chen, C.-Y., Kung, C.-W., 2020. Pore-Confined Silver Nanoparticles in a Porphyrinic Metal–Organic Framework for Electrochemical Nitrite Detection. ACS Appl Nano Mater 3, 9440–9448. https://doi.org/10.1021/acsanm.0c02052

Wang, Z., Wang, X., Ke, C., 2014. Bioaccumulation of trace metals by the live macroalga Gracilaria lemaneiformis. J Appl Phycol 26, 1889–1897. https://doi.org/10.1007/s10811-013-0222-1

Zhang, L., Wang, W.-X., 2023. Silver nanoparticle toxicity to the larvae of oyster Crassostrea angulata: Contribution of in vivo dissolution. Science of The Total Environment 858, 159965. https://doi.org/10.1016/j.scitotenv.2022.159965

Zhang, W., Xiao, B., Fang, T., 2018. Chemical transformation of silver nanoparticles in aquatic environments: Mechanism, morphology and toxicity. Chemosphere 191, 324–334. https://doi.org/10.1016/j.chemosphere.2017.10.016

Zhao, J., Li, Y., Wang, X., Xia, X., Shang, E., Ali, J., 2021. Ionic-strength-dependent effect of suspended sediment on the aggregation, dissolution and settling of silver nanoparticles. Environmental Pollution 279, 116926. https://doi.org/10.1016/j.envpol.2021.116926

Zhou, K., Hu, Y., Zhang, L., Yang, K., Lin, D., 2016. The role of exopolymeric substances in the bioaccumulation and toxicity of Ag nanoparticles to algae. Sci Rep 6, 32998. https://doi.org/10.1038/srep32998

Zhou, M., Ge, X., Ke, D.-M., Tang, H., Zhang, J.-Z., Calvaresi, M., Gao, B., Sun, L., Su, Q., Wang, H., 2019. The Bioavailability, Biodistribution, and Toxic Effects of Silica-Coated Upconversion Nanoparticles in vivo. Front Chem 7. https://doi.org/10.3389/fchem.2019.00218

Zimmermann, M., Gerken, L.R.H., Wee, S., Kissling, V.M., Neuer, A.L., Tsolaki, E., Gogos, A., Lukatskaya, M.R., Herrmann, I.K., 2023. X-ray radio-enhancement by Ti3C2Tx MXenes in soft tissue sarcoma. Biomater Sci 11, 7826–7837. https://doi.org/10.1039/D3BM00607G

Zou, X., Li, P., Lou, J., Fu, X., Zhang, H., 2017. Stability of single dispersed silver nanoparticles in natural and synthetic freshwaters: Effects of dissolved oxygen. Environmental Pollution 230, 674–682. https://doi.org/10.1016/j.envpol.2017.07.007

Graphical abstract

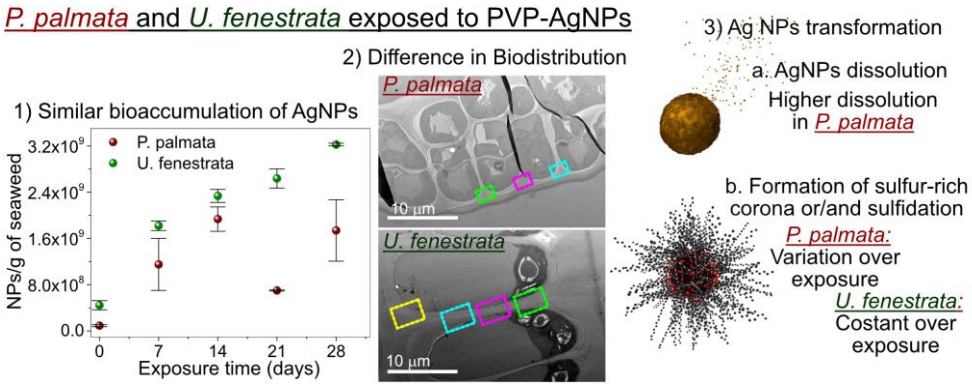

Highlights

- Biodistribution and transformation of silver nanoparticles in edible seaweeds.
- Similar bioaccumulation, ~10^9 NPs/g, in *Ulva fenestrata* and *Palmaria palmata.*
- Biodistribution of silver nanoparticles (AgNPs) heavily depends on the seaweed type.
- Dissolution and sulfur-rich corona; main transformations of AgNPs in seaweed.